Specific binding of Hsp27 and phosphorylated Tau mitigates abnormal Tau aggregation-induced pathology

Shengnan Zhang[1†], Yi Zhu[2†], Jinxia Lu[3†], Zhenying Liu[1,4†], Amanda G Lobato[2,5], Wen Zeng[1,4], Jiaqi Liu[2,6], Jiali Qiang[1], Shuyi Zeng[3], Yaoyang Zhang[1], Cong Liu[1], Jun Liu[7], Zhuohao He[1], R Grace Zhai[2]*, Dan Li[3,8]*

[1]Interdisciplinary Research Center on Biology and Chemistry, Shanghai Institute of Organic Chemistry, Chinese Academy of Sciences, Shanghai, China; [2]Department of Molecular and Cellular Pharmacology, University of Miami Miller School of Medicine, Miami, United States; [3]Bio-X Institutes, Key Laboratory for the Genetics of Developmental and Neuropsychiatric Disorders (Ministry of Education), Shanghai Jiao Tong University, Shanghai, China; [4]University of the Chinese Academy of Sciences, Beijing, China; [5]Graduate Program in Human Genetics and Genomics, University of Miami Miller School of Medicine, Miami, United States; [6]Graduate Program in Molecular and Cellular Pharmacology, University of Miami Miller School of Medicine, Miami, United States; [7]Department of Neurology and Institute of Neurology, Ruijin Hospital, Shanghai Jiao Tong University School of Medicine, Shanghai, China; [8]Zhangjiang Institute for Advanced Study, Shanghai Jiao Tong University, Shanghai, China

*For correspondence:
gzhai@med.miami.edu (RGZ);
lidan2017@sjtu.edu.cn (DL)

[†]These authors contributed equally to this work

Abstract Amyloid aggregation of phosphorylated Tau (pTau) into neurofibrillary tangles is closely associated with Alzheimer's disease (AD). Several molecular chaperones have been reported to bind Tau and impede its pathological aggregation. Recent findings of elevated levels of Hsp27 in the brains of patients with AD suggested its important role in pTau pathology. However, the molecular mechanism of Hsp27 in pTau aggregation remains poorly understood. Here, we show that Hsp27 partially co-localizes with pTau tangles in the brains of patients with AD. Notably, phosphorylation of Tau by microtubule affinity regulating kinase 2 (MARK2), dramatically enhances the binding affinity of Hsp27 to Tau. Moreover, Hsp27 efficiently prevents pTau fibrillation in vitro and mitigates neuropathology of pTau aggregation in a *Drosophila* tauopathy model. Further mechanistic study reveals that Hsp27 employs its N-terminal domain to directly interact with multiple phosphorylation sites of pTau for specific binding. Our work provides the structural basis for the specific recognition of Hsp27 to pathogenic pTau, and highlights the important role of Hsp27 in preventing abnormal aggregation and pathology of pTau in AD.

Editor's evaluation

Phosphorylated Tau (pTau) aggregation into neurofibrillary tangles is closely associated with Alzheimer's disease (AD), and this process is mediated by several molecular chaperones. The authors dissect the important molecular mechanism of the interplay between Hsp27 and pTau, which is relevant to pathology, using a combination of approaches including a *Drosophila* tauopathy model, and biophysical and computational methods. This work provides fundamental molecular insights into the important role of Hsp27 in preventing pTau pathology in AD.

Introduction

Pathological aggregation and propagation of microtubule-associated protein Tau is closely associated with Alzheimer's disease (AD), frontotemporal dementia (FTD), and other tauopathies (*Avila, 2006*; *Hanger et al., 2009*; *Hanger et al., 1998*; *Hanger et al., 1991*; *Spillantini and Goedert, 2013*). Tau is hyper-phosphorylated and forms amyloid fibrils in neurofibrillary tangles (NFT) in patients' brains which is the pathological hallmark of AD. Tau is abundant in the axons of neurons where it stabilizes microtubules (MT; *Drechsel et al., 1992*; *Drubin and Kirschner, 1986*). Under diseased conditions, abnormal phosphorylation of Tau in the regions surrounding the microtubule-binding domain by kinases such as microtubule affinity regulating kinase (MARK) and glycogen synthase kinase 3 (GSK3) leads to dissociation of Tau from MT and subsequent pathological aggregation (*Ando et al., 2016*; *Biernat et al., 1993*; *Drewes, 2004*; *Drewes et al., 1997*; *Hanger et al., 2009*; *Martin et al., 2013*). Moreover, the amyloid fibrils formed by phosphorylated Tau (pTau) have been found to be more potent in mediating the propagation and spread of Tau pathology than those formed by unphosphorylated Tau (*Dujardin et al., 2020*; *Hu et al., 2016*; *Rosenqvist et al., 2018*). Pathological pTau fibrils have been extracted from AD brains, and Hsp27 has been found to co-precipitate with them (*Shimura et al., 2004*). This suggests that Hsp27 may play an important role in pTau pathology.

Hsp27 is a member of the small heat shock protein (sHsp) family which participates in the cellular chaperone network to maintain protein homeostasis by preventing protein abnormal aggregation (*Haslbeck et al., 2005*). It is ubiquitously expressed and plays a protective role in a variety of cellular processes (*Jakob et al., 1993*). Emerging evidence suggests the importance of Hsp27 in AD and other tauopathies. For instance, the expression level of Hsp27 is significantly elevated in affected brain tissues of patients with AD (*Björkdahl et al., 2008*; *Renkawek et al., 1994*), as well as patients with other tauopathies including progressive supranuclear palsy (PSP) and corticobasal degeneration (CBD) (*Schwarz et al., 2010*). Moreover, Hsp27 can effectively inhibit the amyloid aggregation of unphosphorylated Tau in vitro (*Baughman et al., 2018*; *Baughman et al., 2020*; *Freilich et al., 2018*), prevent cellular toxicity of Tau in SH-SY5Y cells (*Choi et al., 2015*), and rescue tauopathies in Tau transgenic mice (*Abisambra et al., 2010*). However, the molecular mechanism of the interplay between Hsp27 and pTau, which exhibits more pathological relevance than that between Hsp27 and unphosphorylated Tau, remains poorly understood.

In this study, we first examined the postmortem brain tissue of patients with AD and detected the co-localization of Hsp27 and pTau aggregates. We next took advantage of a *Drosophila* tauopathy model and uncovered the neuroprotective effects of Hsp27 against pTau-induced synaptopathy in vivo. To dissect the molecular mechanism, we characterized the interaction between Hsp27 and MARK2-mediated hyper-phosphorylated pTau, and the consequent amyloid aggregation in vitro. Employing multiple biophysical and computational approaches, we revealed that Hsp27 recognizes multiple phosphorylation sites of pTau to prevent pTau amyloid aggregation. This work provides molecular insights into the important role of Hsp27 in preventing pTau pathology in AD.

Results

Co-localization of Hsp27 and Tau pathology in human brains with AD

We first asked whether Hsp27 is associated with pathological pTau aggregates in AD brains. We obtained human frontal cortex tissue slices from two cases of AD patients and two cases of age-matched healthy controls (*Table 1*). Immunofluorescence staining using antibodies anti-pTau[Ser262] and anti-Hsp27 detected the presence of pTau in two AD cases, but absent in two healthy controls (*Figure 1*). Notably, Hsp27 was detected at a high level in AD brain slices, but at a much lower or undetectable level in healthy control brain slices (*Figure 1*), consistent with previous findings of elevated Hsp27 levels in AD brains (*Björkdahl et al., 2008*; *Renkawek et al., 1994*). More importantly, Hsp27 was found to co-localize with the pTau aggregates in both AD cases (*Figure 1*), suggesting the pathological relevance between Hsp27 and pTau pathology in AD. Note that not all pTau aggregates contain Hsp27 and vice versa, especially in case 1, which may reflect the heterogeneity of the protein aggregates.

Table 1. Summary of the AD patients and age-matched healthy controls.

Cases	Gender	Age	Brain region	Thal Phase (0–3, Aβ plaques)	Braak stage (0–6, Tau)	CERAD (0–3, neuritic plaque)
AD case 1	F	76	Frontal cortex	3	3	3
AD case 2	F	74	Frontal cortex	3	3	3
Normal case 1	M	77	Frontal cortex	0	0	0
Normal case 2	F	75	Frontal cortex	0	0	0
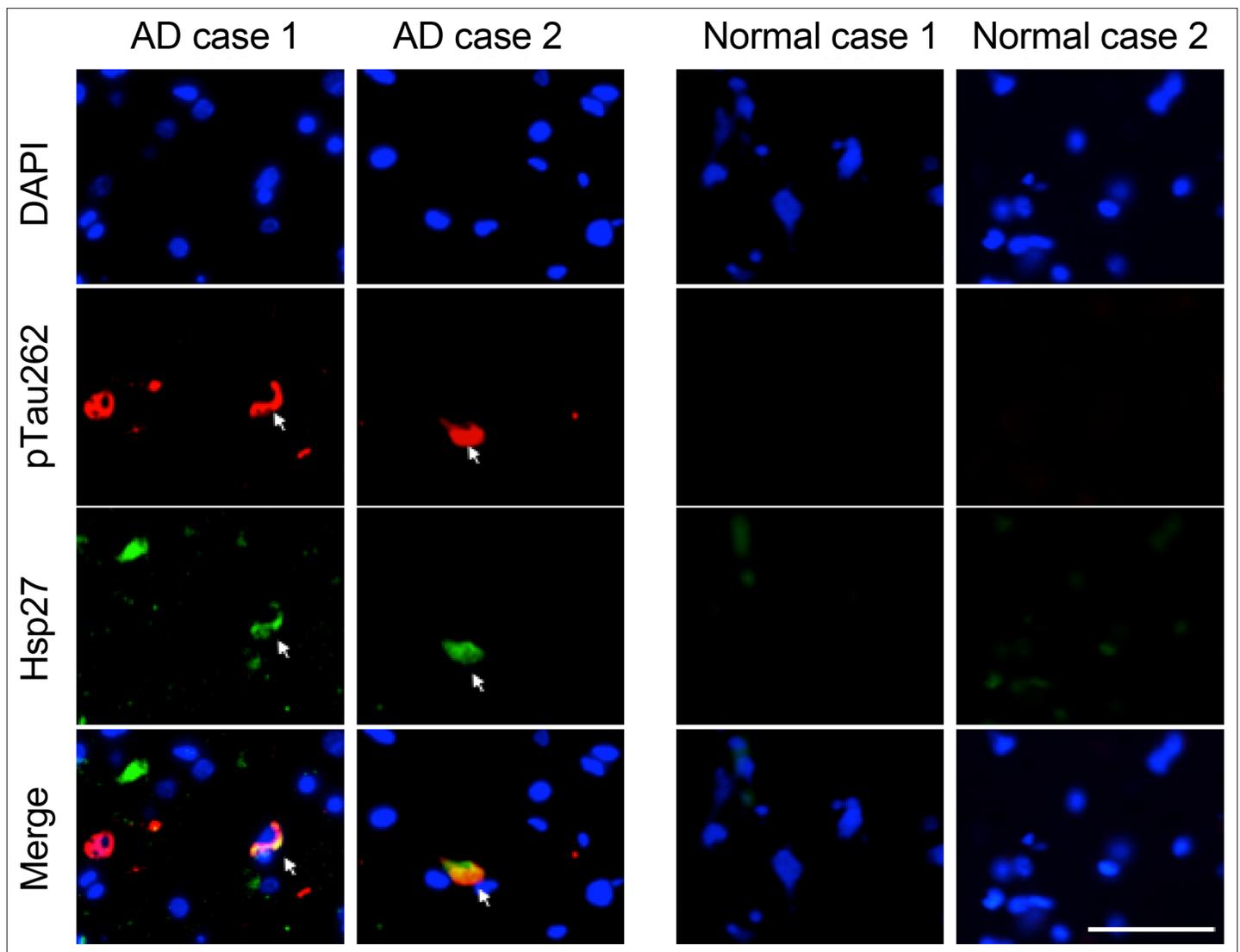
Figure 1. Hsp27 partially co-localizes with pTau aggregates in the brains of AD patients. Representative images of immunofluorescence staining using anti-hyper-phosphorylated Tau at Ser262 and anti-Hsp27 antibodies on the brain slices from two AD and two age-matched normal cases. Green, Hsp27; red, pTau^{S262}; blue, DAPI; Scale bar, 50 μm.

Hsp27 protects pTau-induced synaptopathy in *Drosophila*

To investigate the influence of Hsp27 on the abnormal aggregation of pTau and its neuropathology in vivo, we used a *Drosophila* tauopathy model where human pathogenic mutant Tau (Tau^{R406W}), associated with FTD with parkinsonism linked to chromosome 17 (FTDP-17), is expressed in the nervous system by a pan-neuronal driver *elav^{C155}-GAL4*. Our previous work has demonstrated that the expression of human Tau^{R406W} in the *Drosophila* nervous system leads to age-dependent neurodegeneration recapitulating some of the salient features of tauopathy in FTDP-17 (*Ali et al., 2012*; *Ma et al., 2020*). To quantitatively assess the pTau species in the brain, we carried out western blot analysis using a total Tau antibody 5A6 (*Johnson et al., 1997*), a pTau^{Ser262} specific antibody (*Iijima et al., 2010*), and a hyper-phosphorylated Tau antibody AT8 that recognizes hyper-phosphorylation at Ser202 and Thr205 sites (*Goedert et al., 1995*). Hsp27 overexpression significantly reduced hyper-phosphorylated Tau levels 2 and 10 days after eclosion (DAE) (*Figure 2A and B*, *Figure 2—source data 1*; *Figure 2—source data 2*).

We next examined the morphology of the fly brain and the accumulation of hyper-phosphorylated Tau by immunofluorescence staining. We used the AT8 antibody to label hyper-phosphorylated Tau because phosphorylation at Ser202 and Thr205 occurs after the phosphorylation of S262 and
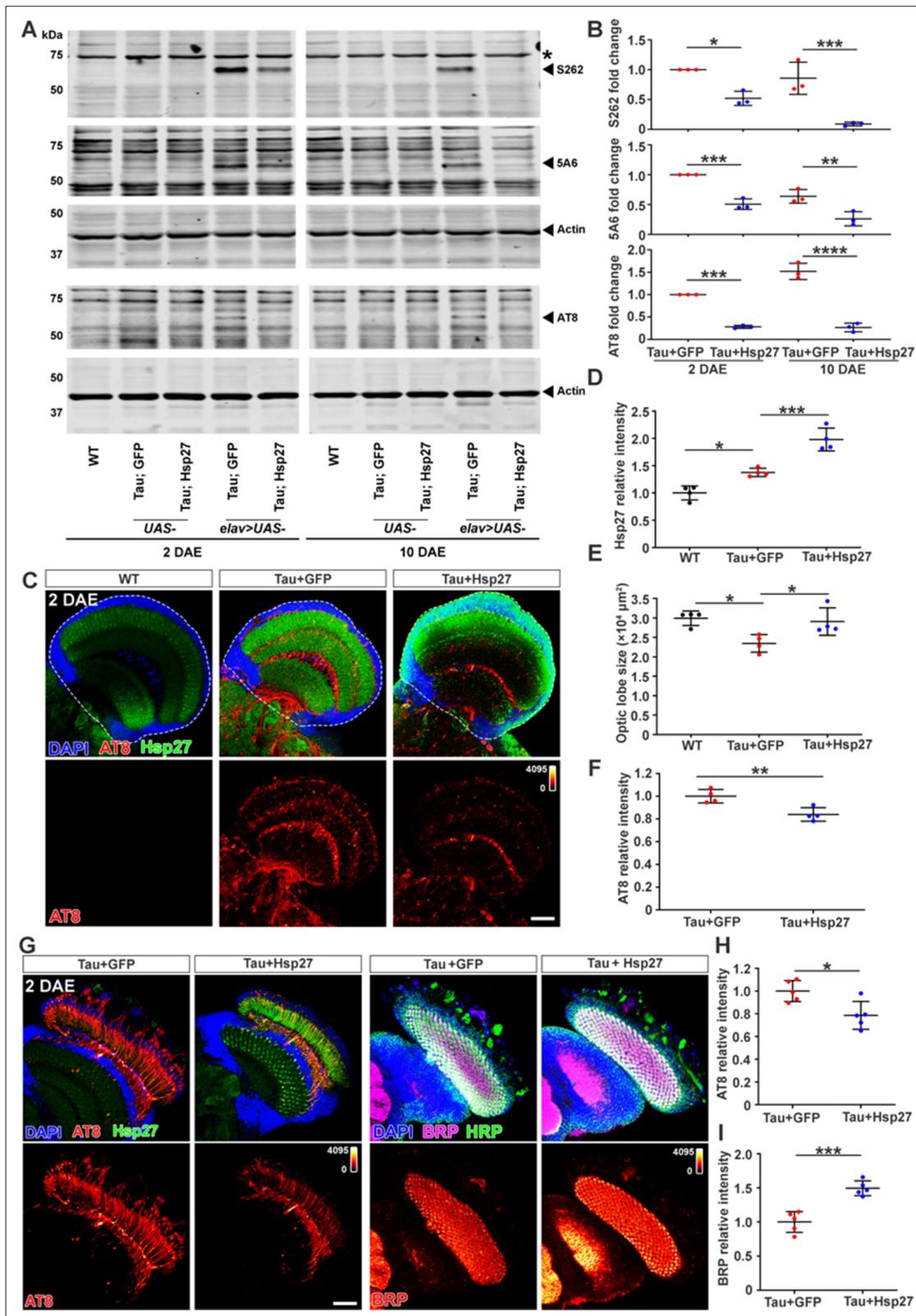
Figure 2. Hsp27 reduces pTau level and protects against pTau-induced synaptopathy in *Drosophila*. (**A**) Brain lysates of 2 and 10 days after eclosion (DAE) wild-type (WT) flies (lanes 1 and 6), flies expressing human Tau with GFP (lanes 4 and 9), or human Tau with Hsp27 (lanes 5 and 10) in the nervous system were probed with antibodies for disease-associated phospho-tau epitopes S262, Ser202/Thr205 (AT8), and total Tau (5A6). Actin was probed as a loading control. Brain lysates of flies carrying only UAS elements were loaded for control (lanes 2, 3, 7, and 8). (**B**) Quantification of protein fold

Figure 2 continued on next page

is associated with advanced pathology (*Wesseling et al., 2020*). Consistent with previous findings, brains with neuronal expression of Tau^{R406W} exhibited an accumulation of filamentous pTau and a reduction of brain neuropil size indicative of neurodegeneration (*Figure 2C–F*). Interestingly, we found that neuronal expression of Tau^{R406W} led to a significant upregulation of endogenous Hsp27, which was highly enriched in the synaptic areas (*Figure 2C and D*), suggesting that Hsp27 might be a part of the neuronal stress response network that is upregulated upon proteotoxic stress. Importantly, overexpression of Hsp27 restored the size of brain neuropil and suppressed the accumulation of filamentous pTau (*Figure 2C–F*), suggesting that Hsp27 protects against mutant Tau^{R406W} induced neurodegeneration.

Synaptic loss is a hallmark of human tauopathy (*McGowan et al., 2006*). To evaluate the synaptic integrity, we took advantage of the *Drosophila* visual system with highly organized paralleled photoreceptor structures (*Fischbach and Dittrich, 1989*). We have previously shown that Tau^{R406W} expression resulted in synaptic aggregation of hyper-phosphorylated Tau as well as a significant reduction of Bruchpilot (Brp), an active zone associated-cytoskeletal matrix protein, at lamina cartridge, suggesting a severe loss of the active zone structures in the presynaptic terminals (*Ma et al., 2020*). As shown in *Figure 2G–I*, we expressed Tau^{R406W} with either GFP (control) or Hsp27 in the photoreceptors using *GMR-GAL4* and found that overexpression of Hsp27 led to a remarkable reduction of synaptic pTau and enhanced BRP localization, indicating a restoration of synaptic integrity.

Taken together, we showed that Hsp27 protects against synaptic dysfunction in a *Drosophila* tauopathy model by reducing pTau aggregation and ameliorating pTau-induced synaptic degeneration.

Hsp27 specifically binds pTau and prevents its amyloid aggregation

We next sought to examine the binding of Hsp27 with pTau and its effect on pTau amyloid aggregation in vitro. We purified the longest Tau isoform – Tau40 that contains both the projection region and four microtubule-binding repeat domains (R1–R4), as well as K19, a truncated Tau construct that contains R1, R3, and R4 (*Figure 3A*). Then phosphorylated Tau, including pTau40 and pK19, were prepared by phosphorylating purified Tau40 and K19 using kinase MARK2 which was previously identified to be important in mediating pTau pathology in AD (*Ando et al., 2016*; *Drewes, 2004*; *Gu et al., 2013*). Two dimensional (2D) ^{1}H-^{15}N HSQC spectra enable us to monitor each of the MARK2 phosphorylation sites in both pTau40 and pK19. Consistent with previous report (*Schwalbe et al., 2013*), eight MARK2 phosphorylation sites including pS262, pS293, pS305, pS324, pS352, pS356, pS413, and pS416 were identified on the HSQC spectrum of pTau40 (*Figure 3—figure supplement 1A*). Four phosphorylation sites including pS262, pS324, pS352, and pS356 were identified on the HSQC spectrum of pK19 (*Figure 3—figure supplement 1B*). Most of these phosphorylation sites are within the fibril forming core region of Tau, and two of them including pS262 and pS356 have been widely reported to be essential for the detachment of pTau from MT and cause increased toxicity in animal models (*Hanger et al., 1998*; *Hanger et al., 2009*; *Ali et al., 2012*).

We used BioLayer Interferometry (BLI) assay to measure the binding affinity of Hsp27 with pTau and unphosphorylated Tau, respectively. pTau and Tau were immobilized on biosensor tips, and the association and dissociation curves were measured in the presence and absence of various concentrations of Hsp27 to calculate the equilibrium dissociation constant (K_D) between Hsp27 and pTau/Tau. Notably, the K_D value of Hsp27/pTau40 is ~1.58 μM (*Figure 3B*; *Figure 3—source data 1*). The K_D value for Hsp27/pK19 is ~1.98 μM (*Figure 3C*; *Figure 3—source data 1*) which is similar to that of
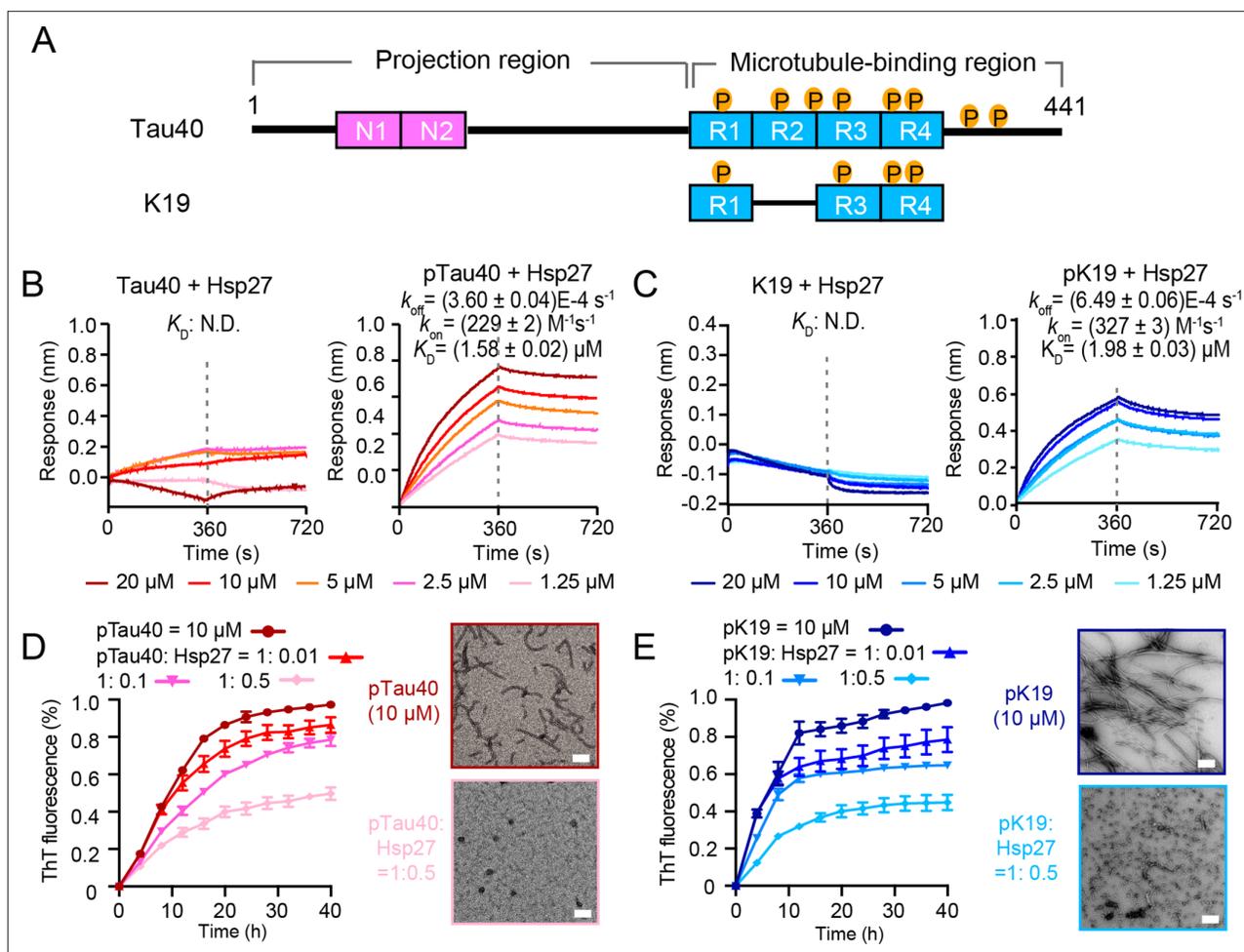
Figure 3. Hsp27 specifically binds MARK2-phosphorylated Tau and prevents its amyloid aggregation. (**A**) Domain schematic of the longest isoform of Tau (Tau40) and a truncated construct K19. Different isoforms of Tau are characterized by 0, 1, or 2 N-terminal insertions (**N1 and N2**), and three (**R1–R3–R4**) or four (**R1-4**) microtubule-binding repeats. The MARK2-phosphorylated sites are indicated. (**B**) Binding affinity of Tau40/pTau40 with Hsp27 determined by BLI. The association and dissociation profiles of Tau40/pTau40 to Hsp27 were divided by a vertical dash line. Tau40/pTau40 was fixed to the sensor, and the 5 concentrations of Hsp27 used are indicated. N.D., not detectable. The determined equilibrium constant (K_D), and the association (k_{on}) and dissociation (k_{off}) rates are labelled. (**C**) Binding affinity of K19/pK19 with Hsp27 determined by BLI. The determined equilibrium constant (K_D), and the association (k_{on}) and dissociation (k_{off}) rates are labelled. (**D&E**) Inhibition of Hsp27 on the amyloid aggregation of 10 μM pTau40 (**D**)/pK19 (**E**) revealed by ThT fluorescence kinetic assay (left) and TEM microscopy (right). A gradient concentration of Hsp27 was applied as indicated. The ThT data showed correspond to mean ± SEM, with n=3 technical replicates. The top and bottom panel on the right are the TEM images of 10 μM pTau40 (**D**)/pK19 (**E**), and 10 μM pTau40 (**D**)/pK19 (**E**) with Hsp27 at a molar ratio of 1:0.5 taken at the end point of the ThT kinetic assay on the left, respectively. Scale bar in TEM images, 50 nm.

The online version of this article includes the following source data and figure supplement(s) for figure 3:

Source data 1. The association and dissociation response of Tau40/pTau40 and K19/pK19 with Hsp27 (**Figure 3B and C**).

Figure supplement 1. 2D ^{1}H-^{15}N HSQC spectra of pTau40 (**A**) and pK19 (**B**) collected at 298 K on a Bruker Avance 900 MHz spectrometer.

Hsp27/pTau40. In addition, both the association (k_{on}) and dissociation (k_{off}) rates of Hsp27 to pK19 are at the same order of magnitude of Hsp27 to pTau40. These results suggest that pK19 serves as the key region for binding of Hsp27 to pTau40. In sharp comparison, the binding of both Hsp27/Tau40 and Hsp27/K19 were much weaker which cannot be detectable under our experimental condition (**Figure 3B and C**; **Figure 3—source data 1**). These results demonstrate that hyper-phosphorylation significantly enhances the binding of Hsp27 to both pTau40 and pK19.

We further assessed the influence of Hsp27 on the amyloid aggregation of pTau40 and pK19 by thioflavin T (ThT) fluorescence assay and negative-staining electron microscopy (EM). The results showed that Hsp27 effectively inhibited the amyloid aggregation of both pTau40 and pK19 in a
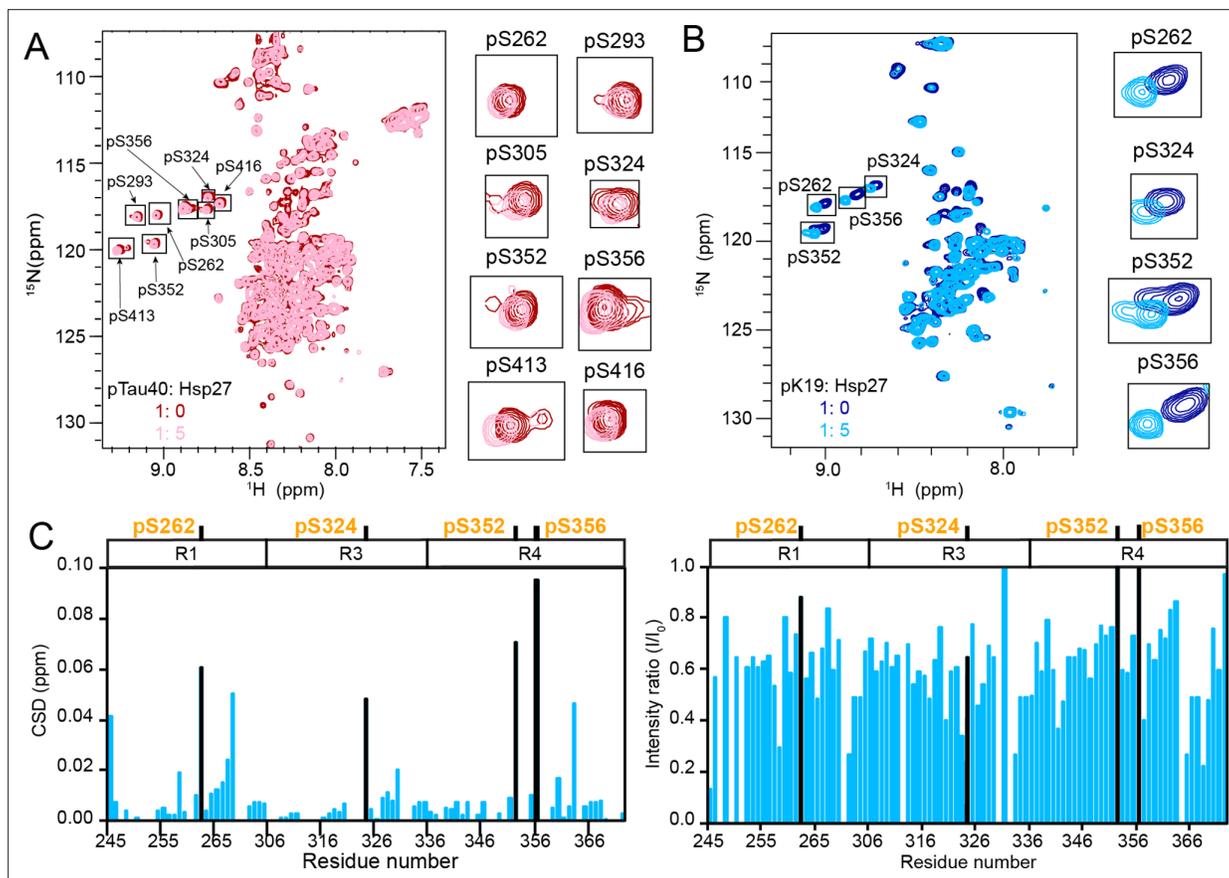
Figure 4. The phosphorylation sites of pTau strongly interact with Hsp27. (A&B) Overlay of the 2D ^{1}H-^{15}N HSQC spectra of 50 μM pTau40 (**A**) and 50 μM pK19 (**B**) in the absence and presence of 250 μM Hsp27. Signals of pSer residues are enlarged and labeled on the right. (**C**) Residue-specific CSDs (left) and intensity changes (right) of pK19 titrated by Hsp27 from (**B**). The domain organization of pK19 is indicated on top and the data of pSer residues are labeled.

The online version of this article includes the following source data and figure supplement(s) for figure 4:

Source data 1. Residue-specific chemical shift changes and intensity changes of pK19 titrated by Hsp27.

Figure supplement 1. Hsp27 interacts very weakly with unphosphorylated Tau.

Figure supplement 1—source data 1. Residue-specific chemical shift changes and intensity changes of K19 titrated by Hsp27.

dose-dependent manner (*Figure 3D and E*; *Figure 3—source data 1*). Together, our data show that Hsp27 can specifically bind to hyper-phosphorylated Tau including pTau40 and pK19, and efficiently prevent their amyloid aggregation.

Hsp27 directly binds to multiple phosphorylation sites of pTau

To investigate the structural basis of the interaction between Hsp27 and pTau, we performed solution NMR spectroscopy, and titrated Hsp27 to ^{15}N-labeled pTau40 and ^{15}N-labeled pK19, respectively. Strikingly, the 2D ^{1}H-^{15}N HSQC spectra showed obvious chemical shift changes (CSDs) of all the eight phosphorylated Ser (pSer) residues of pTau40 and four pSer residues of pK19 upon titration of Hsp27 (*Figure 4A and B*). The highly overlapped signals in the pTau40 HSQC spectrum exclude us to obtain a full assignment of pTau40. Alternatively, we accomplished the backbone assignment of pK19, which enables us to map the binding interface of pK19 with Hsp27. As shown in *Figure 3C*, the regions containing the four pSer residues of pK19 harbor prominent CSDs. Among them, the two pSer residues in R4 showed the largest CSDs above 0.06 ppm (*Figure 4C*; *Figure 4—source data 1*). In addition, titration of Hsp27 to pK19 induced dramatically intensity drops of most residues of pK19 (*Figure 4C*; *Figure 4—source data 1*), implying the direct binding of Hsp27 to pK19 which increases the molecular weight upon pK19-Hsp27 complex formation, and thus increases line width of the cross

peaks. By contrast, addition of the same amount of Hsp27 to unphosphorylated Tau including Tau40 and K19 only results in slightly CSD and intensity perturbations (*Figure 4—figure supplement 1*; *Figure 4—figure supplement 1—source data 1*). Together, our data suggest that phosphorylation of Tau promotes the interaction between Hsp27 and pTau by forming the specific interaction between Hsp27 and the phosphorylated residues of Tau.
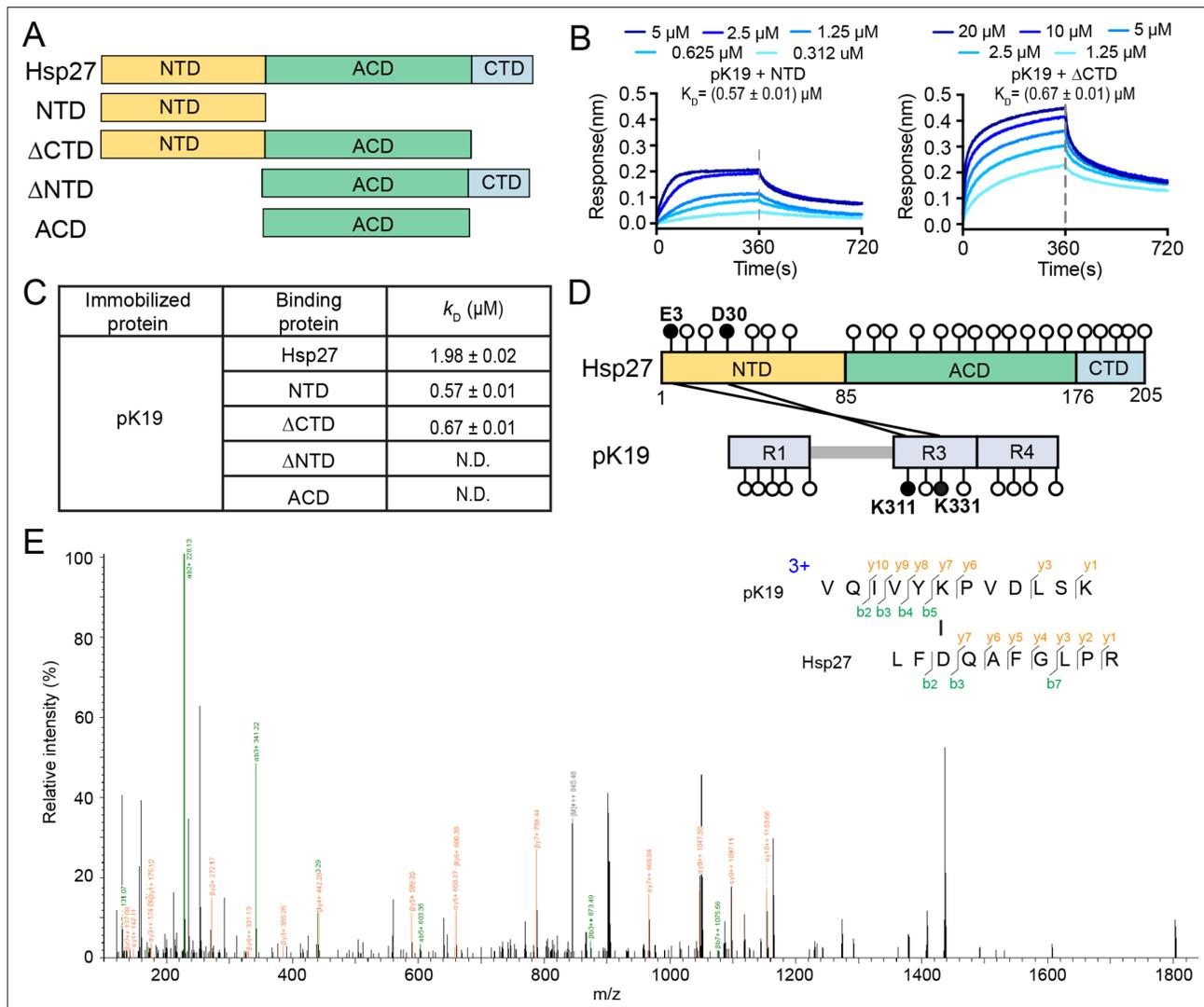
Figure 5. N-terminal domain of Hsp27 is essential in binding with pK19. (**A**) Domain organization of Hsp27 and the four truncations. (**B**) Binding affinity of pK19 with NTD and ΔCTD of Hsp27 determined by BLI. The association and dissociation profiles were divided by a vertical dash line. pK19 was fixed to the sensor, and the 5 concentrations of Hsp27 truncations used are indicated. (**C**) Summary of the binding affinity of pK19 with Hsp27 wild type and truncations. (**D**) Schematic profile of the cross-linked results of Hsp27 to pK19 using cross-linkers EDC and NHS. All GLU (**E**) and ASP (**D**) residues in Hsp27, and all LYS (**K**) residues in pK19 are indicated by circles, respectively. The two identified cross-linked segments are indicated by two black lines and the corresponding residues are highlighted in black circles and labeled. (**E**) A representative MS/MS spectrum of trypsin proteinase-generated peptide. The m/z of fragment ions were matched to their theoretical values generated by in silico fragmentation.

The online version of this article includes the following source data and figure supplement(s) for figure 5:

Source data 1. The association and dissociation response of pK19 with NTD and ΔCTD of Hsp27.

Figure supplement 1. Binding affinity of pK19 with ΔNTD and ACD of Hsp27 determined by BLI.

Figure supplement 1—source data 1. The association and dissociation response of pK19 with ΔNTD and ACD of Hsp27.

Table 2. Cross-linked peptides between pK19 and Hsp27.
The cross-linked residues are bold and underlined in the sequences.

	Peptide sequence (Hsp27-pK19)	Score 1	Score 2	Score 3
1	LF**D**QAFGLPR -VQIVY**K**PVDLSK	2.56246E-11	3.17803E-09	1.21049E-06
2	GSEFENLYFQGMT**E**R-CGSLGNIHH**K**PGGGQVEVK	5.05514E-09	1.37169E-06	9.56423E-07

N-terminal domain (NTD) of Hsp27 mediates the binding of Hsp27 to pTau

Hsp27 composes of a central α-crystallin domain (ACD) flanked by a flexible NTD and a flexible C-terminal domain (CTD). To further dissect the role of different domains of Hsp27 in binding pK19, four different truncations of Hsp27 were prepared (*Figure 5A*). Their binding affinities to pK19 were determined by BLI, respectively. Notably, the isolated NTD binds to pK19 with a K_D value of ~0.57 µM which is similar to the binding affinity of the full-length Hsp27 to pK19 (*Figure 5B*; *Figure 5—source data 1*). ΔCTD which contains both NTD and ACD display a similar binding affinity to pK19 (0.67±0.01 µM; *Figure 5B*; *Figure 5—source data 1*). In contrast, both ACD and ΔNTD which do not contain NTD show no detectable binding to pK19 at the same condition (*Figure 5C* and *Figure 5—figure supplement 1*; *Figure 5—figure supplement 1—source data 1*). Together, these data suggest that Hsp27 NTD plays an essential role in mediating the binding of Hsp27 to pK19.

Next, we performed cross-linking mass spectrometry (CL-MS) to map the interacting regions of Hsp27 and pK19. pK19 was used since it contains less amino acids but keeps the key region of pTau40 for binding Hsp27 to simplify the data analysis. NTD of Hsp27 contains 0 lysine residue. Whereas, negatively charged residues including glutamine acid (E) and aspartic acid (D) evenly distribute within the three different domains of Hsp27 (*Figure 5D*). Thus, we performed a two-step coupling procedure using cross-linkers 1-ethyl-3-(3-dimethylaminopropyl) carbodiimide (EDC) and sulfo-N-hydroxysulfosuccinimide (sulfo-NHS) to cross-link Hsp27 and pK19. EDC causes direct conjugation of carboxylates (-COOH) to primary amines (-NH$_2$) of target molecules, and sulfo-NHS is introduced for stabilization. We identified two pairs of cross-linked segments between Hsp27 and pK19 with a confidence score of $<10^{-6}$ by mass spectrometry, including E3$_{Hsp27}$-K331$_{pK19}$ and D30$_{Hsp27}$-K311$_{pK19}$ (*Figure 5D and E* and *Table 2*). Notably, both cross-linked segments are formed by residues located at R3 of pK19 and NTD of Hsp27 (*Figure 5D*), which is consistent with our NMR titration that residues at R3 show slightly stronger intensity drop upon addition of Hsp27, and the domain truncation mapping results. Together, our data demonstrate that NTD is essential to mediate pK19 binding.

Different domains of Hsp27 bind distinct regions of pK19 to prevent its fibrillation

To further pinpoint the binding regions of pK19 by NTD and other domains of Hsp27, we titrated full-length and the four truncations of Hsp27 to ^{15}N-labeled pK19 and collected a series of HSQC spectra. Titration of both NTD and ΔCTD induce significant CSDs mainly located on the four pSer sites of pK19 (*Figure 6A and B*; *Figure 6—source data 1*), which recapitulates that titrated by full-length Hsp27. In contrast, titration of ACD or ΔNTD caused much smaller CSDs on the four pSer sites of pK19. Moreover, addition of NTD and ΔCTD induces overall intensity drops of pK19 signals (~$I/I_0<0.8$), while titration of ACD and ΔNTD only cause slightly intensity drops. These results demonstrate that Hsp27 mainly uses its NTD to directly interact with the pSer residues of pK19 for pTau binding, which is consistent with the BLI results.

Notably, we found that despite that titration of ACD does not induce CSDs of the pSer sites, it causes relative small but detectable CSDs (>0.01 ppm) and intensity drops ($I/I_0<0.7$) of the highly amyloidogenic region - ^{306}VQIVYK^{311} of pK19, especially residues V309, Y310, and K311 (*Figure 6A and B*; *Figure 6—source data 1*). This demonstrates that ACD is capable of directly binding to pK19 via its VQIVYK region. Of note, the cross peaks of V306, Q307, and I308 severely overlapped with a few residues of pK19 which excludes us to obtain the accurate CSD and intensity changes upon titration. Together, our results demonstrate that different domains of Hsp27 display distinct binding
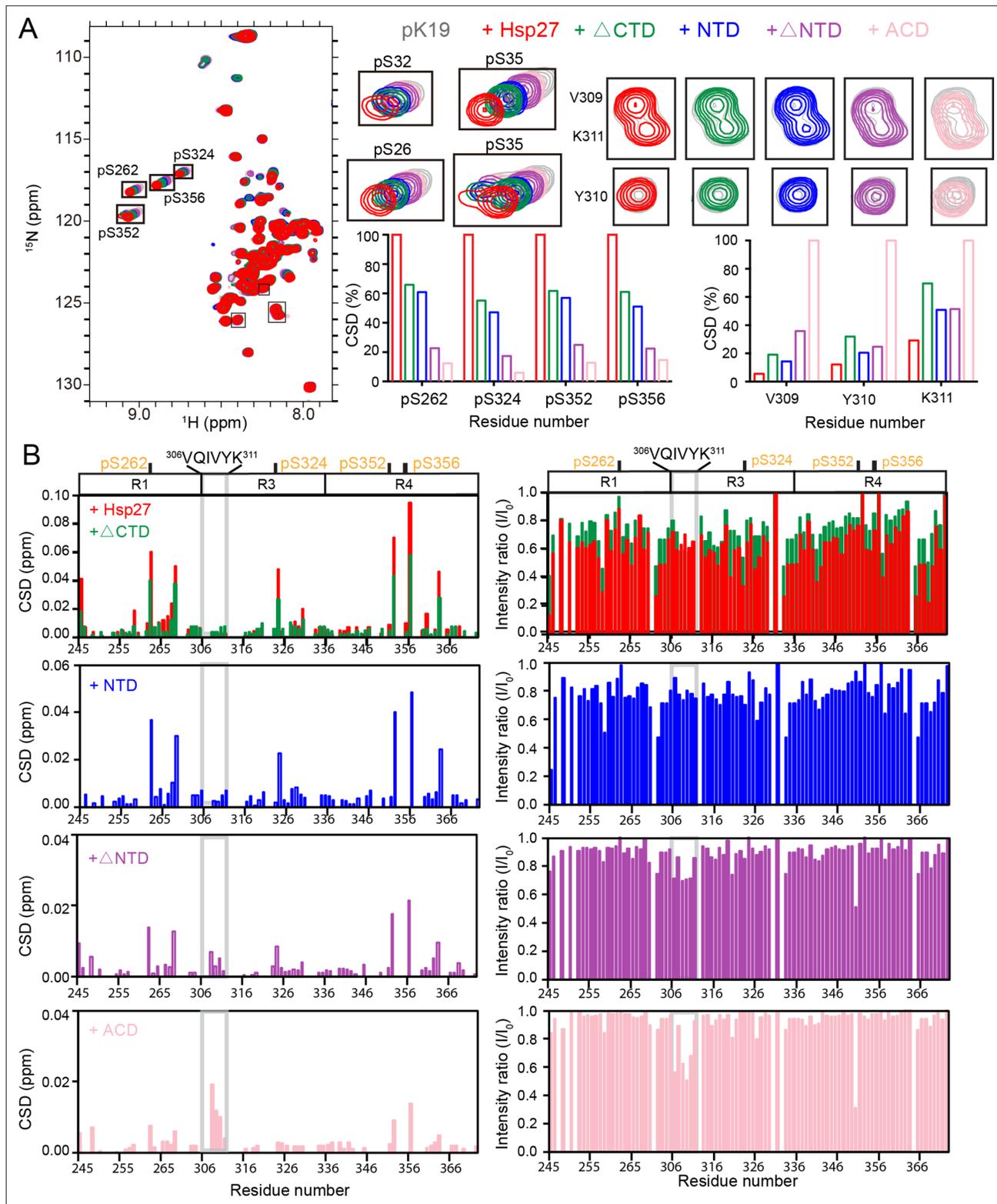
Figure 6. Interaction between pK19 and different domains of Hsp27. (**A**) Overlay of the 2D ^1H-^{15}N HSQC spectra of 50 µM pK19 in the absence and presence of 100 µM Hsp27 variants as indicated. Signals of the four pSer residues and residues V309, Y310, and K311 are labeled and enlarged on the right. Relative CSDs of the four pSer residues and residues V309, Y310, and K311 of pK19 titrated by Hsp27 variants are shown on the right. (**B**) Residue-specific CSDs (left) and intensity changes (right) of pK19 titrated by Hsp27 variants from (**A**). Domain organization of pK19 is indicated on top and the pSer residues are indicated. The amyloidogenic ^{306}VQIVYK^{311} region of pK19 was labeled and highlighted by light gray lines.

Figure 6 continued on next page

preferences to different regions of pK19. NTD exhibits a high binding affinity to the multiple pSer sites of pK19, while ACD weakly binds the amyloidogenic VQIVYK segment of pK19.

Finally, we examined the role of different domains of Hsp27 in preventing amyloid aggregation of pK19 and pTau40. As shown in *Figure 7A and B* (*Figure 7—source data 1*), NTD-containing Hsp27 variants including full-length Hsp27, ΔCTD, and NTD exhibits potent inhibitory activity in preventing both pTau40 and pK19 fibrillation. This suggests that strong binding of NTD to the phosphorylated sites of pTau is important in preventing pTau fibrillation. Interestingly, ACD and ΔNTD display weakened but not negligible inhibitory activity of pTau, especially for pK19. This suggests that binding of ACD to the VQIVYK segment of pTau may result in moderate inhibition of pTau fibrillation. Together, our data show that the NTD is predominately employed to bind pTau to prevent its fibrillation, while ACD also contributes chaperone activity to a less degree by binding to the highly aggregation-prone VQIVYK region of pTau.
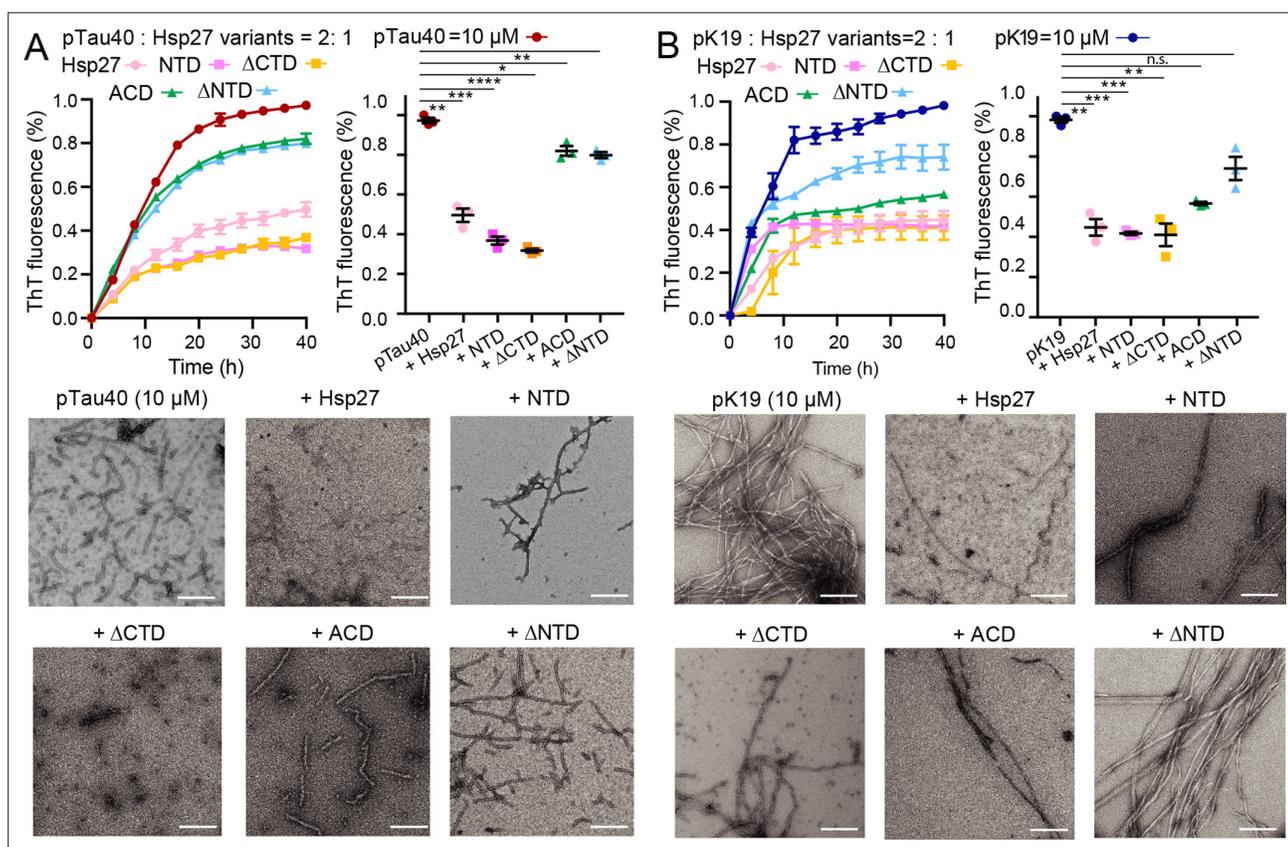
Figure 7. Different domains of Hsp27 play distinctive roles in preventing pTau amyloid aggregation. (**A&B**) Inhibition of Hsp27 variants on the amyloid aggregation of 10 μM pTau40 (**A**)/pK19 (**B**) revealed by ThT fluorescence kinetic assay (top) and TEM microscopy (bottom). The ThT data showed correspond to mean ± s.d., with n=3 technical replicates. Comparison of the inhibitory effect of Hsp27 variants on pTau aggregation at 40 hr time point is shown on the right. p Values based on two-sided Student's t-test. *p<0.05, **p<0.01, ***p<0.001, ****p<0.0001, n.s., not significant. Scale bar in TEM images, 200 nm.

The online version of this article includes the following source data for figure 7:

Discussion

Molecular chaperones play essential roles in maintaining protein homeostasis and preventing protein misfolding and aggregation. Accumulating evidence showed that many molecular chaperones including Hsp70, DnaJA2, Hsp90, Hsp27, and NMNAT can directly interact with Tau and are involved in different steps of Tau biogenesis, aggregation, and clearance (*Baughman et al., 2018*; *Freilich et al., 2018*; *Ma et al., 2020*; *Mok et al., 2018*; *Petrucelli et al., 2004*). Since Hsp27 was identified to co-precipitate with AD brain-derived pTau aggregates and is elevated in AD brains (*Björkdahl et al., 2008*; *Renkawek et al., 1994*; *Shimura et al., 2004*), Hsp27 may play an important role in interacting with pTau in AD. Indeed, we showed elevated Hsp27 levels and partial co-localization of Hsp27 with pTau aggregates in AD brains. More importantly, we found that MARK2-mediated phosphorylation of Tau dramatically increases the binding of pTau to Hsp27, strengthening the notion that Hsp27 binds specifically to disease-related pTau. This specific binding enables Hsp27 to be a potent chaperone in inhibiting amyloid aggregation of MARK2-mediated phosphorylated Tau in vitro.

Over 58 different phosphorylation sites including MARK2-phosphorylation sites were identified on Tau40 in AD brains (*Hanger et al., 1998*; *Hanger et al., 2007*; *Hasegawa et al., 1992*; *Morishima-Kawashima et al., 1995*; *Wesseling et al., 2020*; *Xia et al., 2021*). Phosphorylation at different sites is believed to be involved in different stages of pTau pathology in AD (*Hanger et al., 2009*; *Wesseling et al., 2020*; *Xia et al., 2021*). A previous study examined the inhibitory activity of different chaperons to unmodified Tau and Tau carrying single-point mutations at different phosphorylation sites including S356E, T153E, T231E, S396E, and S404E (*Mok et al., 2018*). Among them, only S356 belongs to MARK2-phosphorylation sites (*Figure 4A*). Strikingly, Hsp27 exhibits potent inhibitory activity on S356E Tau but not the other Tau phosphomimetics (*Mok et al., 2018*). This suggests the binding specificity of Hsp27 on different phosphorylation sites of Tau. It will be important to further explore whether Hsp27 recognizes the other disease-related phosphorylation sites in addition to those modified by MARK2. Moreover, other molecular chaperones including Hsp90 and NMNAT were also found to mediate pTau cellular clearance and prevent pTau aggregation both in vitro and in cells (*Dickey et al., 2007*; *Ma et al., 2020*). The important questions that remained to be addressed include: (1) whether different chaperones preferentially recognize Tau with different phosphorylation patterns; (2) how different chaperones coordinate to prevent disease-related pTau aggregation and pathology.

Hsp27 contains three domains including NTD, ACD, and CTD. We showed in this study that Hsp27 uses its NTD to strongly bind to the multiple phosphorylation sites of pTau. Meanwhile, ACD of Hsp27 transiently and weakly interacts with the highly amyloidogenic region - ^{306}VQIVYK^{311} of pTau. Therefore, different domains of Hsp27 are responsible for binding to distinct regions of pTau. Notably, previous studies showed that, as for the unphosphorylated Tau, ACD exhibits the strongest binding ability by predominantly binding the ^{306}VQIVYK^{311} region of Tau via its β4 and β8 region (*Baughman et al., 2018*; *Baughman et al., 2020*; *Freilich et al., 2018*). While NTD displays much weaker binding to unmodified Tau (*Baughman et al., 2020*; *Freilich et al., 2018*). Therefore, phosphorylation of Tau shifts the paradigm of Hsp27 binding pattern of Tau, which results in significantly enhanced overall binding of Hsp27 to pTau. As the phosphorylation pattern of pTau is dynamically changed upon the progression of AD (*Hanger et al., 2009*; *Wesseling et al., 2020*; *Xia et al., 2021*), how phosphorylation at different sites influences the interplay between pTau and its binding patterns including Hsp27 and different molecular chaperones will be interesting to investigate.

This study demonstrates that NTD of Hsp27 is essential for binding to the phosphorylation sites of pTau. Notably, Hsp27 was found to be phosphorylated at multiple sites on NTD under stress conditions, which leads to dissociation of Hsp27 from high-molecular-weight oligomers to smaller ones with higher chaperone activities (*Alderson et al., 2019*; *Jovcevski et al., 2017*; *Jovcevski et al., 2015*; *Lambert et al., 1999*; *Rogalla et al., 1999*). Our previous work showed that NTD phosphorylation provides an additional layer for regulating Hsp27 activity in controlling the phase separation and amyloid fibrillation of ALS-associated FUS (*Liu et al., 2020*). Whether Hsp27 NTD is phosphorylated under the disease conditions of AD, FTD, and other tauopathies, and how Hsp27 NTD phosphorylation influences the binding and chaperone activity of Hsp27 to pTau are both worthy of being further explored to fully appreciate the complicated interplay between pTau and Hsp27 in disease. Nevertheless, our study demonstrates the important role of Hsp27 in chaperoning pathological pTau from abnormal aggregation, and implies that activating Hsp27 or elevating its level might be a potential strategy for AD treatment.

Materials and methods

Human brain samples and immunofluorescence

Human brain samples were originally from the tissue bank of the Center for Neurodegenerative Disease Research (CNDR) at the University of Pennsylvania. 10% neutral buffered formalin (NBF)-fixed, paraffin-embedded human frontal cortex tissues from two AD patients and two age-matched normal controls were sectioned into 6 µm slices, and immunostained as described before (*He et al., 2018*). Briefly, after deparaffinization and rehydration, the brain slices were incubated with anti-human Hsp27 (1:200, Cat. # ab2790) and anti-pTau^{Ser262} (1:200, Cat. # ab131354) antibodies overnight at 4 °C followed by a 2 hr incubation of Alexa Fluor-conjugated secondary antibodies (Thermo Fisher Scientific), and then mounted with DAPI-containing Fluoromount-G (SouthernBiotech, USA).

Drosophila stocks and genetics

The following fly strains were used: *UAS-Hsp27* (generated in this study); *UAS-Tau^{R406W}* obtained from Dr. Mel Feany (*Wittmann et al., 2001*); *yw*, *UAS-GFP*, *elav-GAL4*, *GMR-GAL4* obtained from Bloomington *Drosophila* Stock Center. Flies were reared on cornmeal-molasses-yeast medium at 22°C, 65% humidity, with 12 hr light/12 hr dark cycles.

Western blot

For protein extraction in flies, 10 heads of each group were homogenized in radioimmunoprecipitation assay (RIPA) buffer (Sigma-Aldrich, R0278). Samples were mixed with Laemmli sample buffer containing 2% SDS, 10% glycerol, 62.5 mM Tris-HCl (pH 6.8), 0.001% bromophenol blue, and 5% β-mercaptoethanol, and heated at 95 °C for 10 min. Proteins were separated by SDS-polyacrylamide gel electrophoresis and transferred to a nitrocellulose membrane. After blocking at room temperature for 1.5 hr, the membrane was incubated with primary antibody at 4 °C overnight, followed by secondary antibody for 1.5 hr at room temperature. Imaging was performed on an Odyssey Infrared Imaging system (LI-COR Biosciences) and analyzed using Image Studio (ver 4.0). Primary antibody dilutions were used as follows: anti-pTau$^{Ser202/Thr205}$ (AT8, 1:500; ThermoScientific, Rockford, IL, USA), anti-pTau^{Ser262} (1:1000; ThermoScientific), anti-β-actin (1:5000, Sigma-Aldrich, St Louis, MO, USA), anti-total-Tau (5A6, 1:250, Developmental Studies Hybridoma Bank, Iowa City, IA, USA).

Fly brain dissection, immunostaining, and confocal microscopy

Fly brains were dissected in phosphate-buffered saline (PBS, pH 7.4) and fixed with 4% formaldehyde at room temperature for 10 min. After 10 min washing in PBTx (PBS containing 0.4% v/v Triton X-100) three times, brains were incubated with primary antibodies diluted in PBTx with 5% normal goat serum at 4 °C overnight. Fly brains were incubated with conjugated secondary antibodies at room temperature for 1 hr, followed by 4′,6- diamidino-2-phenylindole (DAPI, 1:300, Invitrogen, Carlsbad, CA, USA) staining for 15 min. Brains were mounted on slides with VECTASHIELD Antifade Mounting Medium (Vector Laboratories Inc, Burlingame, CA, USA). After that, brains were imaged using an Olympus IX81 confocal microscope coupled with a 60×oil immersion objective lens with a scan speed of 8.0 µs per pixel and spatial resolution of 1024×1024 pixels. Images were processed using FluoView 10-ASW (Olympus) and Adobe Photoshop CS6 and quantified using Fiji/Image J (ver 1.52). Primary antibody dilutions were used as follows: anti-pTau$^{Ser202/Thr205}$ (AT8, 1:250), anti-BRP (nc82, 1:250, Developmental Studies Hybridoma Bank), anti-Hsp27 (1:250, Abcam, Cambridge, MA, USA). The experimenter was blinded to the genotype during confocal scans. The sample size was not predetermined by statistical calculations, but the number of flies and independent biological replicates were large enough to achieve sufficient statistical power, according to our previous publications (*Ma et al., 2020*; *Zhu et al., 2019*). All the data were included in the final analysis.

Plasmid construction for in vitro study

All plasmids used in this study are available upon request. Genes of full-length human Hsp27 (UniProt accession number P04792), and the truncations of Hsp27 including NTD (residues of 1–84), ΔCTD (residues of 1–176), ΔNTD (residues of 85–205), and ACD (residues of 85–175) were inserted into a pET-28a vector with an N-terminal His$_6$-tag and a following tobacco etch virus (TEV) protease cleavage site. Sequencing of all constructs was verified by GENEWIZ company (Suzhou, China).

Protein expression and purification

All proteins were expressed in *Escherichia coli* BL21(DE3) cells, grown to an OD_{600} of 0.8 and induced with 0.3 mM IPTG overnight at 16 °C. Hsp27 and its variants were purified with HisTrapFF column (GE Healthcare) with the Tris buffer (50 mM Tris-HCl, 100 mM NaCl, a gradient of 0~500 mM imidazole, pH 8.0). The N-terminal His_6-tag was removed using TEV protease in the buffer of 50 mM Tris-HCl, 100 mM NaCl, pH 8.0. The cleaved proteins were immediately loaded onto the size-exclusion chromatography column Superdex 75 26/60 (GE Healthcare) with a PBS buffer of 50 mM sodium phosphate, 50 mM NaCl at pH 7.0.

Human Tau40 and K19 were over-expressed and purified as previously described (*Barghorn et al., 2005*). Briefly, Tau/K19 was purified by a HighTrap HP SP (5 ml) column (GE Healthcare), and followed by a Superdex 75 gel filtration column (GE Healthcare).

For ^{15}N-labeled proteins, protein expression was the same as that for unlabeled proteins except that the cells were grown in M9 minimal medium with $^{15}NH_4Cl$ (1 g l^{-1}). Purification of ^{15}N-labeled proteins was the same as that of the unlabeled proteins.

The purity of proteins was assessed by SDS-PAGE. Protein concentration was determined by BCA assay (Thermo Fisher).

In vitro phosphorylation of Tau40/K19

Phosphorylation of Tau40/K19 by MARK2 kinase was carried out following a method described previously (*Ma et al., 2020*). Briefly, Tau40/K19 was incubated with cat MARK2-T208E at a molar ratio of 10:1 in a buffer of 50 mM Hepes, pH 8.0, 150 mM KCl, 10 mM $MgCl_2$, 5 mM ethylene glycol tetraacetic acid (EGTA), 1 mM PMSF, 1 mM dithio-threitol (DTT), 2 mM ATP (Sigma), and protease inhibitor cocktail (Roche) at 30 °C overnight. pTau40/pK19 was further purified by HPLC (Agilent) to remove kinase, and lyophilized. The sites of phosphorylation were quantified using 2D ^1H-^{15}N HSQC spectrum according to previous publications (*Schwalbe et al., 2013*).

NMR spectroscopy

All NMR experiments were performed at 298 K in the NMR buffer of 50 mM sodium phosphate, 50 mM NaCl, and 10% (v/v) D_2O at pH 7.0. 3D HNCA and HNCACB experiments were collected on an Agilent 600 MHz spectrometer for backbone assignment of K19, while 3D HNCA, HNCOCA, CBCACONH, and HNCACB experiments were collected for backbone assignment of pK19. NMR titrations were performed on a Bruker 900 M or Agilent 800 MHz spectrometer. Each sample (500 μl) was made of 50 μM ^{15}N-pTau40/pK19/Tau40/K19, in the absence or presence of Hsp27 and its variants at the indicated concentrations. Intensity changes were calculated by I/I_0. And chemical shift deviations (CSDs, Δδ) were calculated using equation,

$$\Delta\delta = \sqrt{\left(\Delta\delta 1H\right)^2 + 0.0289\left(\Delta\delta 15N\right)^2}$$

Where Δδ1H and Δδ15N are the chemical shift differences of amide proton and amide nitrogen between free and bound state of the protein, respectively. All NMR spectra were processed using NMRPipe (*Delaglio et al., 1995*), and analyzed using Sparky (*Lee et al., 2015*) and NMRView (*Johnson, 2004*).

BioLayer interferometry (BLI) assay

The binding kinetics of the Tau proteins to Hsp27 WT and variants were measured by BLI on an ForteBio Octet RED96 system (Pall ForteBio LLC). Experiments were performed at room temperature using the assay buffer of 50 mM sodium phosphate, 50 mM NaCl, pH 7.0. Tau proteins including pTau40, Tau40, pK19, and K19 were firstly biotinylated by incubating 0.5–1 mg/ml proteins with biotin at a molar ratio of protein: biotin of 2:3 at 4 °C for 30 min, then the excess biotins were removed by desalting column (Zeba Spin Desalting Columns, Thermo). Then biotinylated Tau proteins were immobilized onto streptavidin biosensors (ForteBio) individually, and incubated with varying concentrations of Hsp27 WT and variants as indicated in the figure. The kinetic experiments were performed following the protocol previously (*Zhang et al., 2021*), in which an auto-inhibition step was used to eliminate the non-specifically binding of Hsp27 and its variants to biosensors. The resulting curves were corrected using the blank reference and analyzed by the ForteBio Data Analysis software 9.0.

ThT fluorescence assay

ThT kinetics of pTau/pK19 in the absence and presence of Hsp27 and its variants were recorded using a Varioskan Flash Spectral Scanning Multimode Reader (Thermo Fisher Scientific) with sealed 384-microwell plates (Greiner Bio-One). The assay buffer is 30 mM PBS, 2 mM MgCl2, 1 mM DTT, 0.05% NaN$_3$, pH 7.4. 0.5% (v/v) of fibril seeds (the seeds were prepared by sonicating fibrils for 15 s) were added to promote the fibril formation of pTau/pK19. ThT fluorescence with a final ThT concentration of 30 μM in each sample was measured in triplicates with shaking at 600 *rpm* at 37 °C with excitation at 440 nm and emission at 485 nm.

Transmission electron microscopy (TEM)

Five μl of samples were applied to fresh glow-discharged 300-mesh copper carbon grids and stained with 3% v/v uranyl acetate. Specimens were examined by using Tecnai G2 Spirit TEM operated at an accelerating voltage of 120 kV. Images were recorded using a 4K × 4K charge-coupled device camera (BM-Eagle, FEI Tecnai).

Cross-linking mass spectrometry analysis

Cross-linking experiments were modified from the protocol previously (*Gong et al., 2015*). 0.4 mg EDC (final concentration of ~2 mM) and 1.1 mg Sulfo-NHS (final concentration of ~5 mM) were added to 1 ml of Hsp27 solution and reacted for 15 mins at room temperature. Then 1.4 μl 2-mercaptoethanol (final concentration of 20 mM) was added to quench the activity of EDC. Then pK19 was added to the reaction system at an equal molar ratio with Hsp27, and the proteins were allowed to react for 2 hr at room temperature. Then Tris was added to the reaction system with a final concentration of 50 mM to quench the reaction. Cross-linking products were analyzed by SDS-PAGE to assess the cross-linking efficiency. Before MS analysis, proteins were precipitated with acetone; the pellet was resuspended in 8 M urea, 100 mM Tris (pH 8.5) and digested with trypsin at room temperature overnight. The resulting peptides were analyzed by online nanoflow liquid chromatography tandem mass spectrometry (LC−MS/MS). And the mass spectrometry data were analyzed by pLink (*Yang et al., 2012*).

Additional information

Funding

Author contributions

Shengnan Zhang, Conceptualization, Data curation, Formal analysis, Methodology, Writing – original draft, Writing – review and editing; Yi Zhu, Data curation, Formal analysis, Methodology, Writing – original draft, Writing – review and editing; Jinxia Lu, Zhenying Liu, Conceptualization, Data curation, Formal analysis, Methodology, Writing – original draft; Amanda G Lobato, Jiaqi Liu, Jiali Qiang, Shuyi Zeng, Data curation, Formal analysis; Wen Zeng, Data curation, Formal analysis, Writing – review and editing; Yaoyang Zhang, Supervision, Methodology; Cong Liu, Dan Li, Conceptualization, Supervision, Funding acquisition, Investigation, Project administration, Writing – review and editing; Jun Liu, Formal analysis, Writing – review and editing; Zhuohao He, Resources, Supervision, Investigation, Writing – review and editing; R Grace Zhai, Supervision, Funding acquisition, Investigation, Project administration, Writing – review and editing

Author ORCIDs

Shengnan Zhang (ID) http://orcid.org/0000-0003-1051-7196
Yi Zhu (ID) http://orcid.org/0000-0002-1778-8880
Amanda G Lobato (ID) http://orcid.org/0000-0002-4218-7817
Cong Liu (ID) http://orcid.org/0000-0003-3425-6672
R Grace Zhai (ID) http://orcid.org/0000-0002-7599-1430
Dan Li (ID) http://orcid.org/0000-0002-1609-1539

Ethics

Human subjects: Post-mortem human brain tissue sections were gifted from the Brain bank of the Center for Neurodegenerative Disease Research (CNDR) at the University of Pennsylvania with material transfer agreement and necessary sample information. The tissues were collected at CNDR following a standard procedure, which can be referred to Toledo et al., Alzheimer's & Dementia, 10 (2014) 477-484. The use of those samples was approved by the Ethical committee at Interdisciplinary Research Center on Biology and Chemistry, Chinese Academy of Sciences.

Decision letter and Author response

Decision letter https://doi.org/10.7554/eLife.79898.sa1
Author response https://doi.org/10.7554/eLife.79898.sa2

Additional files

Supplementary files

• MDAR checklist

Data availability

All data generated or analysed during this study are included in the manuscript and supporting file; source data files have been provided for Figures 2–7.

References

Abisambra JF, Blair LJ, Hill SE, Jones JR, Kraft C, Rogers J, Koren J, Jinwal UK, Lawson L, Johnson AG, Wilcock D, O'Leary JC, Jansen-West K, Muschol M, Golde TE, Weeber EJ, Banko J, Dickey CA. 2010. Phosphorylation dynamics regulate hsp27-mediated rescue of neuronal plasticity deficits in tau transgenic mice. *The Journal of Neuroscience* **30**:15374–15382. DOI: https://doi.org/10.1523/JNEUROSCI.3155-10.2010, PMID: 21084594

Alderson TR, Roche J, Gastall HY, Dias DM, Pritišanac I, Ying J, Bax A, Benesch JLP, Baldwin AJ. 2019. Local unfolding of the HSP27 monomer regulates chaperone activity. *Nature Communications* **10**:1068. DOI: https://doi.org/10.1038/s41467-019-08557-8, PMID: 30842409

Ali YO, Ruan K, Zhai RG. 2012. NMNAT suppresses tau-induced neurodegeneration by promoting clearance of hyperphosphorylated tau oligomers in a *Drosophila* model of tauopathy. *Human Molecular Genetics* **21**:237–250. DOI: https://doi.org/10.1093/hmg/ddr449, PMID: 21965302

Ando K, Maruko-Otake A, Ohtake Y, Hayashishita M, Sekiya M, Iijima KM. 2016. Stabilization of microtubule-unbound tau via tau phosphorylation at ser262/356 by par-1/MARK contributes to augmentation of AD-related phosphorylation and aβ42-induced tau toxicity. *PLOS Genetics* **12**:e1005917. DOI: https://doi.org/10.1371/journal.pgen.1005917, PMID: 27023670

Avila J. 2006. Tau phosphorylation and aggregation in alzheimer's disease pathology. *FEBS Letters* **580**:2922–2927. DOI: https://doi.org/10.1016/j.febslet.2006.02.067, PMID: 16529745

Barghorn S, Biernat J, Mandelkow E. 2005. Purification of recombinant tau protein and preparation of alzheimer-paired helical filaments in vitro. *Methods in Molecular Biology* **299**:35–51. DOI: https://doi.org/10.1385/1-59259-874-9:035, PMID: 15980594

Baughman HER, Clouser AF, Klevit RE, Nath A. 2018. HspB1 and hsc70 chaperones engage distinct tau species and have different inhibitory effects on amyloid formation. *The Journal of Biological Chemistry* **293**:2687–2700. DOI: https://doi.org/10.1074/jbc.M117.803411, PMID: 29298892

Baughman HER, Pham T-HT, Adams CS, Nath A, Klevit RE. 2020. Release of a disordered domain enhances hspb1 chaperone activity toward tau. *PNAS* **117**:2923–2929. DOI: https://doi.org/10.1073/pnas.1915099117, PMID: 31974309

Biernat J, Gustke N, Drewes G, Mandelkow EM, Mandelkow E. 1993. Phosphorylation of ser262 strongly reduces binding of tau to microtubules: distinction between PHF-like immunoreactivity and microtubule binding. *Neuron* **11**:153–163. DOI: https://doi.org/10.1016/0896-6273(93)90279-z, PMID: 8393323

Björkdahl C, Sjögren MJ, Zhou X, Concha H, Avila J, Winblad B, Pei J-J. 2008. Small heat shock proteins hsp27 or alphab-crystallin and the protein components of neurofibrillary tangles: tau and neurofilaments. *Journal of Neuroscience Research* **86**:1343–1352. DOI: https://doi.org/10.1002/jnr.21589, PMID: 18061943

Choi S, Oh JH, Kim H, Nam SH, Shin J, Park JS. 2015. Protective effect of tat PTD-hsp27 fusion protein on tau hyperphosphorylation induced by okadaic acid in the human neuroblastoma cell line SH-SY5Y. *Cellular and Molecular Neurobiology* **35**:1049–1059. DOI: https://doi.org/10.1007/s10571-015-0199-1, PMID: 25990227

Delaglio F, Grzesiek S, Vuister GW, Zhu G, Pfeifer J, Bax A. 1995. NMRPipe: a multidimensional spectral processing system based on UNIX pipes. *Journal of Biomolecular NMR* **6**:277–293. DOI: https://doi.org/10.1007/BF00197809, PMID: 8520220

Dickey CA, Kamal A, Lundgren K, Klosak N, Bailey RM, Dunmore J, Ash P, Shoraka S, Zlatkovic J, Eckman CB, Patterson C, Dickson DW, Nahman NS Jr, Hutton M, Burrows F, Petrucelli L. 2007. The high-affinity HSP90-CHIP complex recognizes and selectively degrades phosphorylated tau client proteins. *The Journal of Clinical Investigation* **117**:648–658. DOI: https://doi.org/10.1172/JCI29715, PMID: 17304350

Drechsel DN, Hyman AA, Cobb MH, Kirschner MW. 1992. Modulation of the dynamic instability of tubulin assembly by the microtubule-associated protein tau. *Molecular Biology of the Cell* **3**:1141–1154. DOI: https://doi.org/10.1091/mbc.3.10.1141, PMID: 1421571

Drewes G, Ebneth A, Preuss U, Mandelkow EM, Mandelkow E. 1997. MARK, a novel family of protein kinases that phosphorylate microtubule-associated proteins and trigger microtubule disruption. *Cell* **89**:297–308. DOI: https://doi.org/10.1016/s0092-8674(00)80208-1, PMID: 9108484

Drewes G. 2004. MARKing tau for tangles and toxicity. *Trends in Biochemical Sciences* **29**:548–555. DOI: https://doi.org/10.1016/j.tibs.2004.08.001, PMID: 15450610

Drubin DG, Kirschner MW. 1986. Tau protein function in living cells. *The Journal of Cell Biology* **103**:2739–2746. DOI: https://doi.org/10.1083/jcb.103.6.2739, PMID: 3098742

Dujardin S, Commins C, Lathuiliere A, Beerepoot P, Fernandes AR, Kamath TV, De Los Santos MB, Klickstein N, Corjuc DL, Corjuc BT, Dooley PM, Viode A, Oakley DH, Moore BD, Mullin K, Jean-Gilles D, Clark R, Atchison K, Moore R, Chibnik LB, et al. 2020. Tau molecular diversity contributes to clinical heterogeneity in alzheimer's disease. *Nature Medicine* **26**:1256–1263. DOI: https://doi.org/10.1038/s41591-020-0938-9, PMID: 32572268

Fischbach KF, Dittrich APM. 1989. The optic lobe of *Drosophila melanogaster*. I. A golgi analysis of wild-type structure. *Cell and Tissue Research* **258**:441–475. DOI: https://doi.org/10.1007/BF00218858

Freilich R, Betegon M, Tse E, Mok SA, Julien O, Agard DA, Southworth DR, Takeuchi K, Gestwicki JE. 2018. Competing protein-protein interactions regulate binding of hsp27 to its client protein tau. *Nature Communications* **9**:4563. DOI: https://doi.org/10.1038/s41467-018-07012-4, PMID: 30385828

Goedert M, Jakes R, Vanmechelen E. 1995. Monoclonal antibody AT8 recognises tau protein phosphorylated at both serine 202 and threonine 205. *Neuroscience Letters* **189**:167–169. DOI: https://doi.org/10.1016/0304-3940(95)11484-e, PMID: 7624036

Gong Z, Ding Y-H, Dong X, Liu N, Zhang EE, Dong M-Q, Tang C. 2015. Visualizing the ensemble structures of protein complexes using chemical cross-linking coupled with mass spectrometry. *Biophysics Reports* **1**:127–138. DOI: https://doi.org/10.1007/s41048-015-0015-y, PMID: 27340691

Gu GJ, Wu D, Lund H, Sunnemark D, Kvist AJ, Milner R, Eckersley S, Nilsson LNG, Agerman K, Landegren U, Kamali-Moghaddam M. 2013. Elevated MARK2-dependent phosphorylation of tau in alzheimer's disease. *Journal of Alzheimer's Disease* **33**:699–713. DOI: https://doi.org/10.3233/JAD-2012-121357, PMID: 23001711

Hanger DP, Brion JP, Gallo JM, Cairns NJ, Luthert PJ, Anderton BH. 1991. Tau in alzheimer's disease and down's syndrome is insoluble and abnormally phosphorylated. *The Biochemical Journal* **275 (Pt 1)**:99–104. DOI: https://doi.org/10.1042/bj2750099, PMID: 1826835

Hanger DP, Betts JC, Loviny TL, Blackstock WP, Anderton BH. 1998. New phosphorylation sites identified in hyperphosphorylated tau (paired helical filament-tau) from alzheimer's disease brain using nanoelectrospray mass spectrometry. *Journal of Neurochemistry* **71**:2465–2476. DOI: https://doi.org/10.1046/j.1471-4159.1998.71062465.x, PMID: 9832145

Hanger DP, Byers HL, Wray S, Leung KY, Saxton MJ, Seereeram A, Reynolds CH, Ward MA, Anderton BH. 2007. Novel phosphorylation sites in tau from alzheimer brain support a role for casein kinase 1 in disease pathogenesis. *The Journal of Biological Chemistry* **282**:23645–23654. DOI: https://doi.org/10.1074/jbc.M703269200, PMID: 17562708

Hanger DP, Anderton BH, Noble W. 2009. Tau phosphorylation: the therapeutic challenge for neurodegenerative disease. *Trends in Molecular Medicine* **15**:112–119. DOI: https://doi.org/10.1016/j.molmed.2009.01.003, PMID: 19246243

Hasegawa M, Morishima-Kawashima M, Takio K, Suzuki M, Titani K, Ihara Y. 1992. Protein sequence and mass spectrometric analyses of tau in the alzheimer's disease brain. *The Journal of Biological Chemistry* **267**:17047–17054 PMID: 1512244.

Haslbeck M, Franzmann T, Weinfurtner D, Buchner J. 2005. Some like it hot: the structure and function of small heat-shock proteins. *Nature Structural & Molecular Biology* **12**:842–846. DOI: https://doi.org/10.1038/nsmb993, PMID: 16205709

He Z, Guo JL, McBride JD, Narasimhan S, Kim H, Changolkar L, Zhang B, Gathagan RJ, Yue C, Dengler C, Stieber A, Nitla M, Coulter DA, Abel T, Brunden KR, Trojanowski JQ, Lee VM-Y. 2018. Amyloid-β plaques enhance alzheimer's brain tau-seeded pathologies by facilitating neuritic plaque tau aggregation. *Nature Medicine* **24**:29–38. DOI: https://doi.org/10.1038/nm.4443, PMID: 29200205

Hu W, Zhang X, Tung YC, Xie S, Liu F, Iqbal K. 2016. Hyperphosphorylation determines both the spread and the morphology of tau pathology. *Alzheimer's & Dementia* **12**:1066–1077. DOI: https://doi.org/10.1016/j.jalz.2016.01.014, PMID: 27133892

Iijima K, Gatt A, Iijima-Ando K. 2010. Tau ser262 phosphorylation is critical for abeta42-induced tau toxicity in a transgenic *Drosophila* model of alzheimer's disease. *Human Molecular Genetics* **19**:2947–2957. DOI: https://doi.org/10.1093/hmg/ddq200, PMID: 20466736

Jakob U, Gaestel M, Engel K, Buchner J. 1993. Small heat shock proteins are molecular chaperones. *The Journal of Biological Chemistry* **268**:1517–1520. DOI: https://doi.org/10.1016/S0021-9258(18)53882-5, PMID: 8093612

Johnson GV, Seubert P, Cox TM, Motter R, Brown JP, Galasko D. 1997. The tau protein in human cerebrospinal fluid in alzheimer's disease consists of proteolytically derived fragments. *Journal of Neurochemistry* **68**:430–433. DOI: https://doi.org/10.1046/j.1471-4159.1997.68010430.x, PMID: 8978756

Johnson BA. 2004. Using nmrview to visualize and analyze the NMR spectra of macromolecules. *Methods in Molecular Biology* **278**:313–352. DOI: https://doi.org/10.1385/1-59259-809-9:313, PMID: 15318002

Jovcevski B, Kelly MA, Rote AP, Berg T, Gastall HY, Benesch JLP, Aquilina JA, Ecroyd H. 2015. Phosphomimics destabilize hsp27 oligomeric assemblies and enhance chaperone activity. *Chemistry & Biology* **22**:186–195. DOI: https://doi.org/10.1016/j.chembiol.2015.01.001, PMID: 25699602

Jovcevski B, Kelly MA, Aquilina JA, Benesch JLP, Ecroyd H. 2017. Evaluating the effect of phosphorylation on the structure and dynamics of hsp27 dimers by means of ion mobility mass spectrometry. *Analytical Chemistry* **89**:13275–13282. DOI: https://doi.org/10.1021/acs.analchem.7b03328, PMID: 29135234

Lambert H, Charette SJ, Bernier AF, Guimond A, Landry J. 1999. HSP27 multimerization mediated by phosphorylation-sensitive intermolecular interactions at the amino terminus. *The Journal of Biological Chemistry* **274**:9378–9385. DOI: https://doi.org/10.1074/jbc.274.14.9378, PMID: 10092617

Lee W, Tonelli M, Markley JL. 2015. NMRFAM-SPARKY: enhanced software for biomolecular NMR spectroscopy. *Bioinformatics* **31**:1325–1327. DOI: https://doi.org/10.1093/bioinformatics/btu830, PMID: 25505092

Liu Z, Zhang S, Gu J, Tong Y, Li Y, Gui X, Long H, Wang C, Zhao C, Lu J, He L, Li Y, Liu Z, Li D, Liu C. 2020. Hsp27 chaperones FUS phase separation under the modulation of stress-induced phosphorylation. *Nature Structural & Molecular Biology* **27**:363–372. DOI: https://doi.org/10.1038/s41594-020-0399-3, PMID: 32231288

Ma X, Zhu Y, Lu J, Xie J, Li C, Shin WS, Qiang J, Liu J, Dou S, Xiao Y, Wang C, Jia C, Long H, Yang J, Fang Y, Jiang L, Zhang Y, Zhang S, Zhai RG, Liu C, et al. 2020. Nicotinamide mononucleotide adenylyltransferase uses its NAD^+ substrate-binding site to chaperone phosphorylated tau. *eLife* **9**:e51859. DOI: https://doi.org/10.7554/eLife.51859, PMID: 32250733

Martin L, Latypova X, Wilson CM, Magnaudeix A, Perrin ML, Yardin C, Terro F. 2013. Tau protein kinases: involvement in alzheimer's disease. *Ageing Research Reviews* **12**:289–309. DOI: https://doi.org/10.1016/j.arr.2012.06.003, PMID: 22742992

McGowan E, Eriksen J, Hutton M. 2006. A decade of modeling alzheimer's disease in transgenic mice. *Trends in Genetics* **22**:281–289. DOI: https://doi.org/10.1016/j.tig.2006.03.007, PMID: 16567017

Mok S-A, Condello C, Freilich R, Gillies A, Arhar T, Oroz J, Kadavath H, Julien O, Assimon VA, Rauch JN, Dunyak BM, Lee J, Tsai FTF, Wilson MR, Zweckstetter M, Dickey CA, Gestwicki JE. 2018. Mapping interactions with the chaperone network reveals factors that protect against tau aggregation. *Nature Structural & Molecular Biology* **25**:384–393. DOI: https://doi.org/10.1038/s41594-018-0057-1, PMID: 29728653

Morishima-Kawashima M, Hasegawa M, Takio K, Suzuki M, Yoshida H, Titani K, Ihara Y. 1995. Proline-directed and non-proline-directed phosphorylation of PHF-tau. *The Journal of Biological Chemistry* **270**:823–829. DOI: https://doi.org/10.1074/jbc.270.2.823, PMID: 7822317

Petrucelli L, Dickson D, Kehoe K, Taylor J, Snyder H, Grover A, De Lucia M, McGowan E, Lewis J, Prihar G, Kim J, Dillmann WH, Browne SE, Hall A, Voellmy R, Tsuboi Y, Dawson TM, Wolozin B, Hardy J, Hutton M. 2004. CHIP and hsp70 regulate tau ubiquitination, degradation and aggregation. *Human Molecular Genetics* **13**:703–714. DOI: https://doi.org/10.1093/hmg/ddh083, PMID: 14962978

Renkawek K, Bosman GJ, de Jong WW. 1994. Expression of small heat-shock protein hsp 27 in reactive gliosis in alzheimer disease and other types of dementia. *Acta Neuropathologica* **87**:511–519. DOI: https://doi.org/10.1007/BF00294178, PMID: 8059604

Rogalla T, Ehrnsperger M, Preville X, Kotlyarov A, Lutsch G, Ducasse C, Paul C, Wieske M, Arrigo AP, Buchner J, Gaestel M. 1999. Regulation of hsp27 oligomerization, chaperone function, and protective activity against oxidative stress/tumor necrosis factor alpha by phosphorylation. *The Journal of Biological Chemistry* **274**:18947–18956. DOI: https://doi.org/10.1074/jbc.274.27.18947, PMID: 10383393

Rosenqvist N, Asuni AA, Andersson CR, Christensen S, Daechsel JA, Egebjerg J, Falsig J, Helboe L, Jul P, Kartberg F, Pedersen LØ, Sigurdsson EM, Sotty F, Skjødt K, Stavenhagen JB, Volbracht C, Pedersen JT. 2018. Highly specific and selective anti-ps396-tau antibody C10.2 targets seeding-competent tau. *Alzheimer's & Dementia* **4**:521–534. DOI: https://doi.org/10.1016/j.trci.2018.09.005, PMID: 30386817

Schwalbe M, Biernat J, Bibow S, Ozenne V, Jensen MR, Kadavath H, Blackledge M, Mandelkow E, Zweckstetter M. 2013. Phosphorylation of human tau protein by microtubule affinity-regulating kinase 2. *Biochemistry* **52**:9068–9079. DOI: https://doi.org/10.1021/bi401266n, PMID: 24251416

Schwarz L, Vollmer G, Richter-Landsberg C. 2010. The small heat shock protein HSP25/27 (hspb1) is abundant in cultured astrocytes and associated with astrocytic pathology in progressive supranuclear palsy and corticobasal degeneration. *International Journal of Cell Biology* **2010**:717520. DOI: https://doi.org/10.1155/2010/717520, PMID: 20150973

Shimura H, Miura-Shimura Y, Kosik KS. 2004. Binding of tau to heat shock protein 27 leads to decreased concentration of hyperphosphorylated tau and enhanced cell survival. *The Journal of Biological Chemistry* **279**:17957–17962. DOI: https://doi.org/10.1074/jbc.M400351200, PMID: 14963027

Spillantini MG, Goedert M. 2013. Tau pathology and neurodegeneration. *The Lancet. Neurology* **12**:609–622. DOI: https://doi.org/10.1016/S1474-4422(13)70090-5, PMID: 23684085

Wesseling H, Mair W, Kumar M, Schlaffner CN, Tang S, Beerepoot P, Fatou B, Guise AJ, Cheng L, Takeda S, Muntel J, Rotunno MS, Dujardin S, Davies P, Kosik KS, Miller BL, Berretta S, Hedreen JC, Grinberg LT, Seeley WW, et al. 2020. Tau PTM profiles identify patient heterogeneity and stages of alzheimer's disease. *Cell* **183**:1699–1713.. DOI: https://doi.org/10.1016/j.cell.2020.10.029, PMID: 33188775

Wittmann CW, Wszolek MF, Shulman JM, Salvaterra PM, Lewis J, Hutton M, Feany MB. 2001. Tauopathy in *Drosophila*: Neurodegeneration without neurofibrillary tangles. Science **293**:711–714. DOI: https://doi.org/10.1126/science.1062382, PMID: 11408621

Xia Y, Prokop S, Giasson BI. 2021. "Don't phos over tau": recent developments in clinical biomarkers and therapies targeting tau phosphorylation in alzheimer's disease and other tauopathies. *Molecular Neurodegeneration* **16**:37. DOI: https://doi.org/10.1186/s13024-021-00460-5, PMID: 34090488

Yang B, Wu Y-J, Zhu M, Fan S-B, Lin J, Zhang K, Li S, Chi H, Li Y-X, Chen H-F, Luo S-K, Ding Y-H, Wang L-H, Hao Z, Xiu L-Y, Chen S, Ye K, He S-M, Dong M-Q. 2012. Identification of cross-linked peptides from complex samples. *Nature Methods* **9**:904–906. DOI: https://doi.org/10.1038/nmeth.2099, PMID: 22772728

Zhang S, Liu YQ, Jia C, Lim YJ, Feng G, Xu E, Long H, Kimura Y, Tao Y, Zhao C, Wang C, Liu Z, Hu JJ, Ma MR, Liu Z, Jiang L, Li D, Wang R, Dawson VL, Dawson TM, et al. 2021. Mechanistic basis for receptor-mediated pathological α-synuclein fibril cell-to-cell transmission in parkinson's disease. *PNAS* **118**:e2011196118. DOI: https://doi.org/10.1073/pnas.2011196118, PMID: 34172566

Zhu Y, Li C, Tao X, Brazill JM, Park J, Diaz-Perez Z, Zhai RG. 2019. Nmnat restores neuronal integrity by neutralizing mutant huntingtin aggregate-induced progressive toxicity. *PNAS* **116**:19165–19175. DOI: https://doi.org/10.1073/pnas.1904563116, PMID: 31484760